2010

On momentum conservation and thermionic emission cooling

Raseong Kim
Birck Nanotechnology Center, Purdue University, kim369@purdue.edu

Changwook Jeong
Birck Nanotechnology Center, Purdue University, jeong.changwook@gmail.com

Mark S. Lundstrom
Purdue University, lundstro@purdue.edu

Kim, Raseong; Jeong, Changwook; and Lundstrom, Mark S., "On momentum conservation and thermionic emission cooling" (2010). *Department of Electrical and Computer Engineering Faculty Publications.* Paper 136.
http://dx.doi.org/10.1063/1.3295899

On momentum conservation and thermionic emission cooling

Raseong Kim,[a] Changwook Jeong, and Mark S. Lundstrom
Network for Computational Nanotechnology, Birck Nanotechnology Center, Purdue University, West Lafayette, Indiana 47907, USA

(Received 7 July 2009; accepted 23 December 2009; published online 2 March 2010)

The possibility of increasing the performance of thermionic cooling devices by relaxing lateral momentum conservation is examined. Upper limits for the ballistic emission current are established. It is then shown that for most cases, nonconserved lateral momentum model produces a current that exceeds this upper limit. For the case of heterojunctions with a much heavier effective mass in the barrier and with a low barrier height, however, relaxing lateral momentum may increase the current. These results can be simply understood from the general principle that the current is limited by the location, well or barrier, with the smallest number of conducting channels. They also show that within a thermionic emission framework, relaxing lateral momentum conservation does not increase the upper limit performance in most cases, and when it does, the increase is modest. More generally, however, especially when the connection to the carrier reservoir is poor and performance is well below the upper limit, relaxing lateral momentum conservation could prove beneficial. © *2010 American Institute of Physics*. [doi:10.1063/1.3295899]

I. INTRODUCTION

Thermionic (TI) cooling is a method of refrigeration with the potential for high cooling power and efficiency.[1–3] As depicted in Fig. 1, it is based on thermionic emission over a potential barrier. (This figure will be revisited in Sec. V.) When carriers with high energy (hot carriers) are injected over the barrier, the carrier distribution in the emitter region becomes out of equilibrium. To restore equilibrium, cold carriers move up and populate higher energy states by absorbing heat from the lattice, and cooling occurs in the region before the emitter-barrier junction.[4,5] The purpose of this paper is to address the question of whether relaxing lateral momentum conservation at the junction can significantly increase the performance of TI cooling devices as has been proposed.[6,7]

The main differences between TI cooling and the more conventional thermoelectric (TE) cooling are the carrier transport mechanism and the operating regime.[8] In TI cooling, carrier transport is treated as ballistic and no joule heating occurs in the channel.[4] In TE cooling, however, transport is assumed to be diffusive, and joule heating is a part of the heat balance.[9] In addition, while TE devices operate in the linear regime with a small voltage difference, TI devices operate in the nonlinear regime with high drain bias to eliminate the carrier injection from the drain and maximize the heat current injected from the source.[10]

Previous theoretical studies have compared the performances of TI and TE cooling devices.[8,11,12] It has been shown that for the same material, TE cooling is better because it gives higher maximum temperature difference $\Delta T_{\max}$ than that obtained from TI cooling.[8] It has been suggested that nonconservation of lateral momentum may increase the number of electrons participating in the thermionic emission process and therefore significantly improve the TI cooling performance,[6,7,10] and adjusting the nonplanar interface has been proposed to realize it.[13,14] Recently, however, a quantum transport simulation with microscopic scattering models reported that momentum relaxation at the rough interface actually decreases the carrier transmission.[15] In this work, we identify a more fundamental limit of performance enhancement due to nonconserved lateral momentum (NCLM). We explore the upper limit of ballistic emission current using an idealized semiclassical model, and the results identify a significant obstacle to realizing the benefits proposed by nonconservation of lateral momentum even in the ideal case.

The paper is organized as follows. In Sec. II, we compare two equivalent approaches to describe carrier injection over the barrier, a top-of-the-barrier (TOB) model, and a thermionic emission model, and review the concept of NCLM. In Sec. III, the general theory of thermionic emission is reviewed, and results are presented for homo- and heterojunctions. In Sec. IV, a simple physical interpretation is provided to explain the results in Sec. III. In Sec. V, we identify conditions for which momentum relaxation can improve performance. Conclusions follow in Sec. VI.

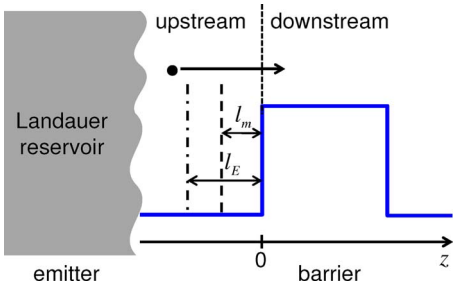

FIG. 1. (Color online) Schematic of a potential barrier connected to a Landauer reservoir (z is the transport direction). When hot carriers are injected over the barrier, cold carriers absorb heat from the lattice and populate higher energy states to restore the equilibrium distribution, and cooling occurs in the region before the emitter-barrier junction. Carrier transport is assumed to be ballistic in this paper, but scattering before the barrier ($z < 0$) may reduce the current below the thermionic emission value (l_E and l_m denote the energy and momentum relaxation lengths).

[a]Electronic mail: kim369@purdue.edu.

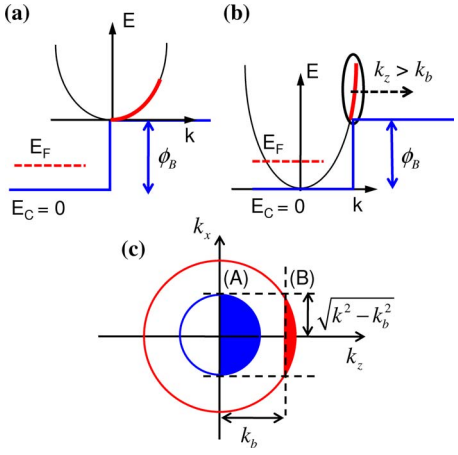

FIG. 2. (Color online) Two approaches that describe carrier injection across homojunctions: (a) TOB model and (b) thermionic emission model. (c) k-space distribution of 3D carriers contributing to the current shown on the k_z-k_x plane with k_y=0. (a) E-k relation is considered in the barrier and the $+k_z$ states are filled according to E_F. (b) E-k relation is considered in the well and carriers with $k_z > k_b$ are injected from the well over the barrier.

II. TOB AND THERMIONIC EMISSION MODELS

In this section, we compare two approaches that describe carrier injection over a barrier, the TOB model[16] and the traditional thermionic emission model.[17] Both models assume ballistic transport and ideal connection to Landauer reservoirs.[18] In the TOB model, the E-k relation is considered in the barrier as shown in Fig. 2(a), and $+k_z$ states (z is the transport direction) are filled according to the source Fermi level E_F. This follows directly from a solution to the ballistic Boltzmann transport equation.[19] In the thermionic emission model,[17] we focus on the well, as shown in Fig. 2(b), and carriers with $k_z > k_b$ are injected from the well over the barrier. The value of k_b is determined by the barrier height ϕ_B, as $k_b = \sqrt{2m^*\phi_B}/\hbar$, where m^* is the carrier effective mass and $\hbar$ is the reduced Planck constant. Note that the conduction band edge E_C, is assumed to be 0 in the well region in Figs. 2(a) and 2(b). The condition $k_z > k_b$ implies that the lateral momentum is conserved during the emission process.

As discussed in the Appendix, the two approaches are equivalent for homojunctions, where m^* is uniform in the well and the barrier region. As an example, Fig. 2(c) shows the k-space distribution (on the k_z-k_x plane with k_y=0) of three-dimensional (3D) carriers that contribute to the current in the TOB picture (A) and thermionic emission picture (B). Then for a single parabolic band, the ballistic electrical and heat currents are given as

$$I_{3D}/A = \frac{qm^*}{2\pi^2\hbar^3}(k_BT)^2\mathcal{F}_1(\eta_F), \tag{1a}$$

$$I_{q,3D}/A = \frac{m^*}{2\pi^2\hbar^3}(k_BT)^3[2\mathcal{F}_2(\eta_F) - \eta_F\mathcal{F}_1(\eta_F)], \tag{1b}$$

where A is the cross-sectional area of the device, q is the unit charge, k_B is the Boltzmann constant, T is the temperature, $\mathcal{F}_j$ is the Fermi–Dirac integral of order j,[20,21] and $\eta_F = (E_F - \phi_B)/k_BT$, which is the reduced Fermi level in the barrier region.

For heterojunction barriers, however, questions arise. For example, it is not clear which effective mass to use in Eq. (1), the well mass m_1^* or the barrier mass m_2^*. Questions also arise if we relax the assumption of conservation of lateral momentum inherent in the conventional thermionic emission approach. It has been suggested that nonconservation of lateral momentum may give higher emission current because all carriers with $k > k_b$ are injected over the barrier while only those with $k_z > k_b$ are injected when the lateral momentum is conserved.[6,7] According to the TOB model, however, $+k_z$ states in the barrier are already in equilibrium with the source and no additional current is possible. In the next section, we review the general theory of thermionic emission across homo- and heterojunctions to address these questions.

III. THERMIONIC EMISSION ACROSS HETEROJUNCTIONS

We begin with a review of the general theory of thermionic emission across heterojunctions as presented by Wu and Yang.[22] It is assumed that m^* changes abruptly at the junction interface.[22–24] Wu and Yang assume that the total energy E and the lateral momentum $\hbar k_\perp$ are conserved

$$E_{\perp,1} + E_{\parallel,1} = E_{\perp,2} + E_{\parallel,2} + \phi_B, \tag{2a}$$

$$m_1^* E_{\perp,1} = m_2^* E_{\perp,2}, \tag{2b}$$

where $E_\perp$ and $E_\parallel$ are the kinetic energies along the lateral and longitudinal (transport) directions, and subscripts 1 and 2 denote the well and the barrier regions, respectively. It can be shown that Eq. (2) guarantees flux continuity across the barrier.[22,24] In this work, we use a semiclassical transmission for simplicity, so the transmission is 1 for carriers satisfying Eq. (2) and 0 otherwise. Using a quantum mechanically computed transmission[22] would not change our conclusions. From now on, we call this approach the "CLM model."

In summary, we have three approaches to describe thermionic emission over the barrier: (1) the conserved lateral momentum (CLM) model, (2) the TOB model, and (3) the NCLM model. In the CLM model, total energy and lateral momentum are conserved as shown in Eq. (2), and the theory applies generally for homo- and heterojunctions. In the TOB model, $+k_z$ states on the barrier are filled according to E_F without considering the injection mechanism from the well. In the NCLM model, carriers with $k > k_b$ are injected from the well without considering the occupation of states in the barrier. Using these three approaches, we examine three cases: (1) homojunction with barrier, (2) heterojunction with no barrier, and (3) heterojunction with barrier. For heterojunctions, we consider two cases: (i) $m_1^* > m_2^*$ and (ii) $m_1^* < m_2^*$. The mathematics of these three cases is discussed in the Appendix; only the results are discussed below.

Results for a homojunction with a barrier are shown in Fig. 3. As discussed in Sec. II and depicted in Fig. 3(a), the CLM and TOB models are equivalent for homojunctions. For the NCLM model in Fig. 3(b), however, it is not clear how to

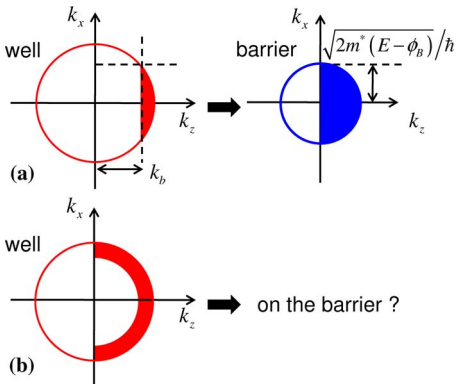

FIG. 3. (Color online) Results for a homojunction with ϕ_B. (a) The CLM model becomes equivalent to the TOB model. (b) It is not clear how the NCLM model can be described in the barrier because states in the barrier are already filled according to E_F.

map the k-states in the well to the barrier. Since all of the states in the barrier are already filled according to E_F, as shown in Fig. 3(a), it does not seem possible for a current in excess of that given by Eq. (1) to flow.

In Fig. 4, we examine the case where m^* changes abruptly, but there is no potential barrier. For such cases, it is well known that the smaller m^* determines the current,[25–27] and the electrical and heat currents are given from Eq. (1) with the lighter m^*. As shown in Fig. 4(a) when $m_1^*>m_2^*$, the current is determined by the states on the right (deep color), so the current is overestimated when all carriers with $k_z>0$ on the left (light color) are assumed to be emitted. When $m_1^*<m_2^*$, the current is determined by the smaller m_1^* on the left (deep color), and the current is overestimated when it is assumed that all carriers with $k_z>0$ on the right (light color) contribute to the current, as shown in Fig. 4(b).

Next, we consider heterojunctions with potential barrier. When $m_1^*>m_2^*$, the CLM model is equivalent to the TOB model, as shown in Fig. 5(a), and the total current is still determined by the lighter m_2^* of the barrier. The current expression for 3D carriers is the same as Eq. (1) with $m^*=m_2^*$. Note that the k-space distribution of carriers in the well that are able to surmount the barrier is different from the homojunction case that was shown in Fig. 3(a). (For details, see

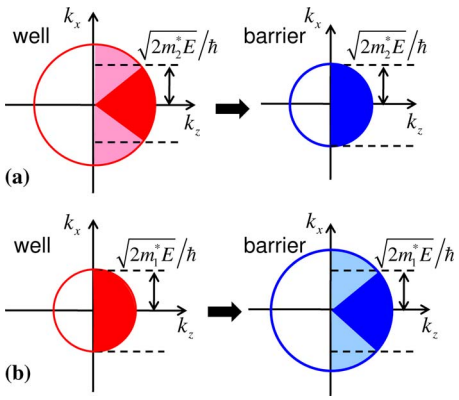

FIG. 4. (Color online) Results for a heterojunction with $\phi_B=0$. The smaller m^* determines the current. (a) When $m_1^*>m_2^*$, the current is determined by the states on the right. (b) When $m_1^*<m_2^*$, the current is determined by the states on the left.

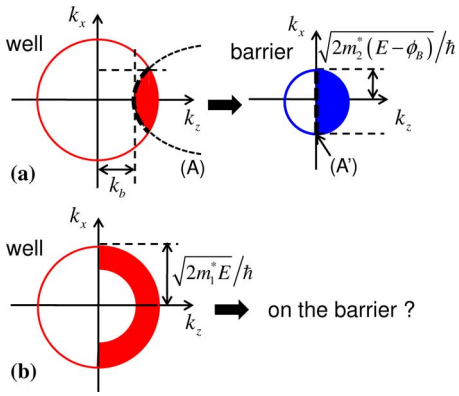

FIG. 5. (Color online) Results for a heterojunction with $m_1^*>m_2^*$ and ϕ_B. (a) The CLM model is equivalent to the TOB model. The hyperbola (A) in the well [Eq. (A3)] is mapped onto the k_x-k_y plane with $k_z=0$ (A′) on the barrier. (b) The results from the NCLM model overestimate the current and cannot be mapped to the barrier.

the Appendix.) Because the CLM model is consistent with the TOB model, the results from the NCLM model in Fig. 5(b) still cannot be mapped from the well to the barrier and would overestimate the ballistic current.

When $m_1^*<m_2^*$ with a potential barrier, there are two competing factors, the barrier height and the magnitude of the lighter effective mass. As discussed in the homojunction case and illustrated in Fig. 3(a), increasing ϕ_B tends to make the barrier states more dominant, while the lighter m_1^* tends to make the well states more dominant as was illustrated in Fig. 4(b). We examine, therefore, two cases: (i) $m_1^*<\sim m_2^*$ with high ϕ_B and (ii) $m_1^*\ll m_2^*$ with low ϕ_B. We expect that the states in the barrier will dominate in case (i) while the well states will in case (ii).

When $m_1^*<\sim m_2^*$ with high ϕ_B, the CLM model is equivalent to the TOB model as shown in Fig. 6(a), and the 3D ballistic current is given as Eq. (1) with $m^*=m_2^*$. It should be noted that the current is determined by the heavier mass m_2^* of the barrier unlike the case with $\phi_B=0$ in Fig. 4(b). Detailed expressions are shown in the Appendix. Because the

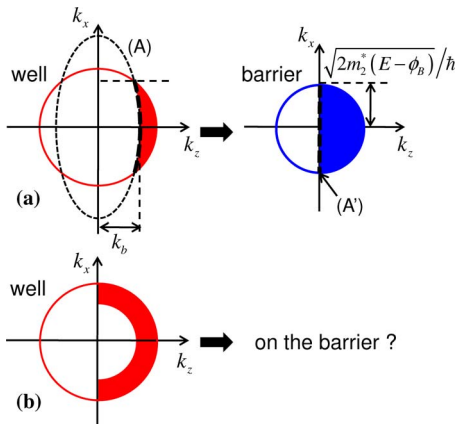

FIG. 6. (Color online) Results for a heterojunction with $m_1^*<\sim m_2^*$ and high ϕ_B. (a) The CLM model is equivalent to the TOB model. The ellipsoid (A) in the well [Eq. (A3)] is mapped onto the k_x-k_y plane with $k_z=0$ (A′) on the barrier. (b) The results from the NCLM model overestimate the current and cannot be mapped to the barrier.

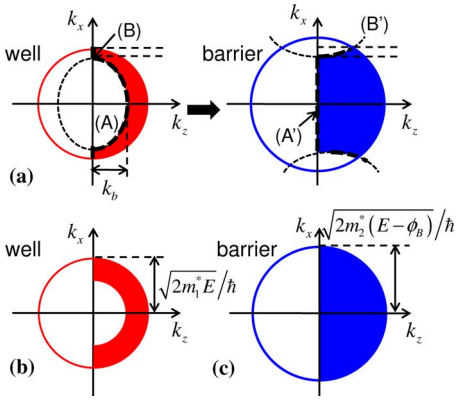

FIG. 7. (Color online) Results for a heterojunction with $m_1^* \ll m_2^*$ and low ϕ_B. (a) The CLM model is different from both the NCLM model and the TOB model. The ellipsoid (A) in the well [Eq. (A3)] is mapped onto the k_x-k_y plane with $k_z=0$ (A′) on the barrier, and the k_x-k_y plane with $k_z=0$ (B) in the well is mapped onto the hyperbola (B′) on the barrier [Eq. (A5)]. (b) The maximum possible current is given by the NCLM model. (c) The TOB model overestimates the current.

current is determined by the states in the barrier, the NCLM model still cannot be mapped to the barrier and would overestimate the current as shown in Fig. 6(b).

The second case, $m_1^* \ll m_2^*$ with low ϕ_B, is examined in Fig. 7. Note that the CLM model in Fig. 7(a) is different from both the NCLM model and the TOB model. (See the Appendix for details.) Note that as shown in Fig. 7(a), the states in the barrier are not completely filled by the source distribution function unlike other cases shown in Figs. 3(a), 5(a), and 6(a). There is, therefore, room for improving the emission current, and the maximum possible current is given by the NCLM model, as shown in Fig. 7(b). The TOB model in Fig. 7(c) overestimates the current because it is larger than the maximum that can be supplied by the well which is given by the NCLM model. In this case, it appears that the proposed increase in TI cooling by relaxing momentum conservation[6,7] could be achieved.

The possible improvement due to nonconservation of lateral momentum when $m_1^* \ll m_2^*$ with low ϕ_B is calculated in Fig. 8. For a model 3D device with $m_1^*=0.25m_0$, $m_2^*=m_0$, $\phi_B=50$ meV, and $T=300$ K, where m_0 is the free electron mass; the improvement of I is about 18% at $\eta_F=-1$, as shown in Fig. 8(a), and it is about 8% for I_q as shown in Fig. 8(b). The improvement is modest because the carrier distributions are already similar in the CLM and NCLM models as shown in Figs. 7(a) and 7(b).

IV. CONDUCTANCE AND MINIMUM NUMBER OF MODES

The results in the previous section can be understood with a simple general rule. Given the numbers of conducting channels (or modes) in the well and the barrier, $M_1(E)$ and $M_2(E)$, the smaller one determines the total conductance.[28] As an example, we consider a 3D heterojunction where the numbers of modes increase linearly with E, and the slope is proportional to m^* as[29]

$$M_1(E) = m_1^* E/2\pi\hbar^2, \tag{3a}$$

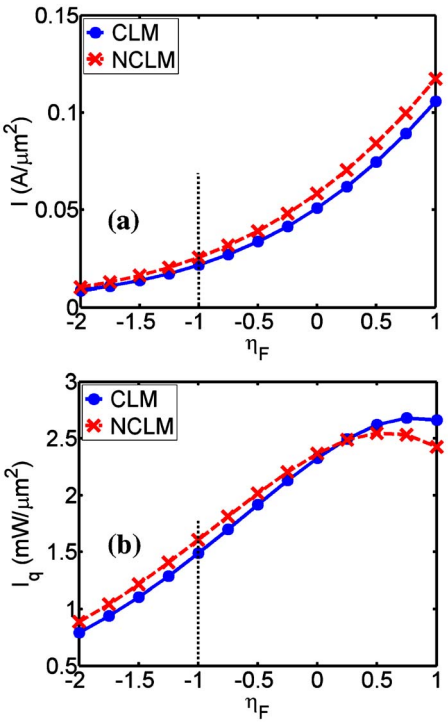

FIG. 8. (Color online) Possible improvement over the CLM model (circle) due to NCLM (cross) for a 3D model device with $m_1^*=0.25m_0$, $m_2^*=m_0$, $\phi_B=50$ meV, and $T=300$ K. (a) The improvement of I is about 18% at $\eta_F=-1$ [Eq. (A6a)]. (b) The improvement of I_q is about 8% at $\eta_F=-1$ [Eq. (A6b)].

$$M_2(E) = m_2^*(E-\phi_B)/2\pi\hbar^2. \tag{3b}$$

Three different cases are considered in Fig. 9. In Fig. 9(a) where $m_1^* > m_2^*$, $M_1(E) > M_2(E)$ regardless of the value of ϕ_B, so $M_2(E)$ determines the conductance. For heterojunctions with $m_1^* < m_2^*$, we consider two cases: (1) $m_1^* < \sim m_2^*$ with high ϕ_B as shown in Fig. 9(b) and (2) $m_1^* \ll m_2^*$ with low ϕ_B, as shown in Fig. 9(c). In Fig. 9(b), although m_2^* in the barrier is heavier, due to the high ϕ_B, $M_2(E)$ is smaller than $M_1(E)$ and determines the current. In Fig. 9(c) for case (2), however, $M_1(E) < M_2(E)$ because the much lighter m_1^* in the well dominates despite the potential barrier, so it is the carrier injection from the well that limits the current. In this case, nonconservation of lateral momentum may help increase the emission current by maximizing the carrier injection from the well.

The results above are summarized in Table I. The TOB model represents an upper limit to the possible current while the NCLM model represents the maximum current that could be supplied by the well if there were states in the barrier to accept them; the minimum of the two determines the current. In many cases, the TOB model gives correct results while the NCLM model overestimates the current. In cases where the number of modes in the well is smaller than that of the barrier ($m_1^* \ll m_2^*$ with low ϕ_B), nonconservation of lateral momentum may increase the emission current.

V. DISCUSSION

As discussed in Sec. III, the TOB model assumes that the carrier distribution in the barrier, $f(E)$, follows the equilib-

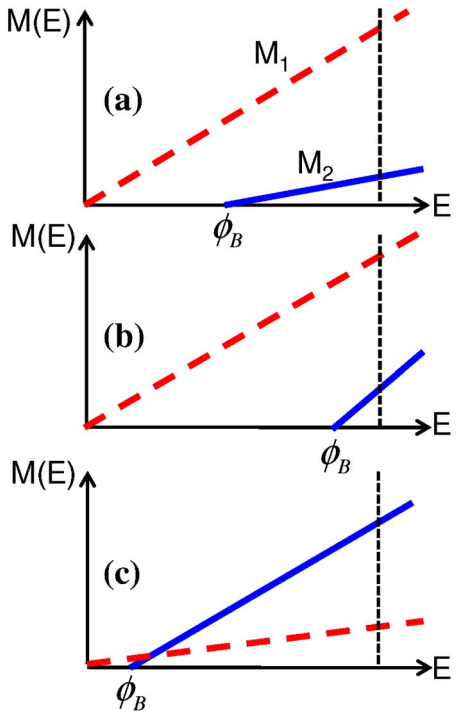

FIG. 9. (Color online) General rule to determine the emission current across heterojunctions. For $M_1(E)$ (dashed line) and $M_2(E)$ (solid line), the smaller one determines the current. (a) When $m_1^* > m_2^*$, $M_1(E) > M_2(E)$ regardless of the value of ϕ_B. (b) When $m_1^* < \sim m_2^*$ with high ϕ_B, although m_2^* is heavier, $M_1(E) > M_2(E)$ due to the high ϕ_B. (c) When $m_1^* \ll m_2^*$ with low ϕ_B, $M_1(E) < M_2(E)$ because the much lighter m_1^* dominates despite ϕ_B.

rium Fermi–Dirac distribution of the source region $f_0(E)$.[16] For cases in Table I where the TOB model is consistent with the CLM model, $f(E)$ must be larger than $f_0(E)$ to achieve the increase in current predicted by the NCLM model, which does not appear to be physically possible. Examples are discussed in the Appendix.

It has been shown that momentum relaxation is essential to interpret the experimental results of ballistic electron emission microscopy (BEEM) for nonepitaxial metal-semiconductor interfaces.[30–32] In BEEM measurements, carriers with small lateral momentum are predominantly injected,[30] but valleys with zero lateral momentum are not preferentially populated as would be expected if lateral momentum were conserved.[30] The observed significant current for the valleys with nonzero lateral momentum indicates that additional lateral momentum is provided by scattering at the nonepitaxial interface.[32] The BEEM measurement results and the theories of nonconservation of lateral momentum used to explain them have motivated the idea that nonconservation of lateral momentum might similarly enhance the emission current and TI cooling performance.[6] The problems are, however, quite different. The critical difference between BEEM experiments and TI cooling devices is that the carrier reservoirs are different. For TI cooling devices, the source reservoir should be designed to act as closely as possible to an ideal Landauer reservoir,[18] where the equilibrium distribution is maintained by a high carrier density, high number of modes, and high scattering rates. Such a reservoir can provide carriers with all possible k's with any given E. For such cases, the NCLM model may be unphysical or give only moderate improvements as discussed in previous sections. In BEEM experiments, however, the reservoir is far from ideal because the lateral momentum of injected carriers is predominantly zero. For such conditions, relaxing lateral momentum may help increase the emission current by shuffling the momentum distribution of carriers and performing the role of scattering in the ideal, Landauer reservoir. The maximum current, however, can never exceed the ballistic limit, which is determined by the minimum number of modes as summarized in Table I.

TABLE I. Summary of the general rule that determines the emission current across heterojunctions. The TOB model represents an upper limit to the possible current while the NCLM model represents the maximum current that could be supplied by the well and the minimum of the two determines the current.

		CLM	TOB	NCLM
Homojunction		Correct	Correct	Incorrect
Heterojunction $m_1^* > m_2^*$		Correct	Correct	Incorrect
Heterojunction $m_1^* < m_2^*$	$m_1^* < \sim m_2^*$, high ϕ_B	Correct	Correct	Incorrect
	$m_1^* \ll m_2^*$, low ϕ_B	Correct	Incorrect	Possible

Monte Carlo simulations[13,14] have shown that adjusting the nonplanar interface structure may enhance the emission by breaking the translational invariance and relaxing lateral momentum conservation. We may interpret this enhancement as a result of the increased effective area.[33] We should note, however, that for devices connected to ideal reservoirs, momentum relaxation at the interface may rather increase carrier backscattering and decrease the emission current. A recent quantum transport simulation with realistic interface roughness[15] shows that in case momentum randomization occurs before the barrier, i.e., the well behaves more like an ideal reservoir, the interface roughness actually decreases the overall transmission probability and the power factor.

Finally, we mention other issues that deserve consideration. We have assumed a ballistic (thermionic emission) model in which all of the scattering occurs in the Landauer reservoirs. In practice, scattering will occur throughout the structure. In the well region before the barrier ($z < 0$ in Fig. 1), momentum or energy relaxing scattering may reduce the current below the thermionic emission value. A similar problem, transport in Schottky barriers, was considered by Bethe[34] and by Berz.[35] Fischetti *et al.*[36] have discussed the source starvation in nanoscale metal-oxide-semiconductor field-effect transistors. The idea is that the longitudinal momentum states that are injected over the barrier can become depleted, and momentum randomizing scattering in the well could help by replenishing these longitudinal k-states. All of these can be labeled "upstream" effects,[37] which occur before the barrier at $z < 0$ in Fig. 1. Fischetti *et al.*[37] also discussed "downstream" effects—scattering in the barrier itself and in the well beyond the barrier, $z > 0$ in Fig. 1. Although they are beyond the scope of this paper, more quantitative studies of the effect of scattering on TI cooling devices will be essential to understand the physics and performance limits of such devices. We also note that our semiclassical model does not work for superlattices with very thin barriers, where the band structure is different from the bulk E-k of its con-

stituent materials, and tunneling becomes significant compared to thermionic emission.[38] Although these are not directly related to the questions involving lateral momentum conservation and the suggested current enhancement, it will be essential to treat quantum transport to explore possible performance enhancements in quantum-engineered TE devices such as superlattices.

VI. CONCLUSIONS

In this paper, we studied the physics of thermionic emission across homo- and heterojunctions to explore the possibilities to increase the emission current and the cooling performance of TI cooling devices. We showed that the TOB model[16] is equivalent to the CLM model[22] for homojunctions, heterojunctions with heavier m^* in the source, and heterojunctions with heavier m^* in the barrier region and high ϕ_B. For such cases, the NCLM model[6] is not consistent with the TOB model and, we believe, overestimates the current that is possible. For heterojunctions with much heavier m^* in the barrier with low ϕ_B, however, we note that nonconservation of lateral momentum may increase the current because there are unfilled states in the barrier when the lateral momentum is conserved. These results can be explained by a simple general rule that given the numbers of modes in the well and the barrier, the overall conductance is determined by the minimum of the two.[28] These results show that within thermionic emission framework, the possibilities of increasing TI cooling by relaxing momentum conservation are limited. For real TI cooling devices, however, as opposed to the ballistic devices connected to ideal, Landauer reservoirs considered here, momentum randomizing scattering in the well may enhance performance and is worth exploring.

ACKNOWLEDGMENTS

This work was supported by the Semiconductor Research Corporation under Research ID 1871 and by National Science Foundation under Grant No. ECS-0609282. Computational support was provided by the Network for Computational Nanotechnology, supported by the National Science Foundation under Cooperative Agreement Grant No. EEC-0634750. It is a pleasure to acknowledge helpful discussions with L. Siddiqui and Professor S. Datta at Purdue University, Professor A. Shakouri at the University of California at Santa Cruz, Dr. S. Jin at Synopsys Inc., and Professor M. V. Fischetti at the University of Massachusetts at Amherst.

APPENDIX: MATHEMATICS OF THE TOB AND WU–YANG MODELS

In the TOB model, the ballistic I and I_q for 3D carriers are calculated as

$$I_{3D,TOB}/A = \frac{q}{4\pi^3}\int_0^\infty dkk^2 \int_0^{\pi/2} d\theta \sin\theta \int_0^{2\pi} d\phi \frac{\hbar k}{m_2^*}\cos\theta f_0 = \frac{qm_2^*}{2\pi^2\hbar^3}(k_BT)^2\mathcal{F}_1(\eta_F), \tag{A1a}$$

$$I_{q,3D,TOB}/A = \frac{1}{4\pi^3}\int_0^\infty dkk^2 \int_0^{\pi/2} d\theta \sin\theta \int_0^{2\pi} d\phi (E - E_F)\frac{\hbar k}{m_2^*}\cos\theta f_0 = \frac{m_2^*}{2\pi^2\hbar^3}(k_BT)^3[2\mathcal{F}_2(\eta_F) - \eta_F\mathcal{F}_1(\eta_F)]. \tag{A1b}$$

Expressions for one-dimensional and two-dimensional (2D) carriers can be obtained in a similar way. We split the CLM model into two cases, $m_1^* > m_2^*$ and $m_1^* < m_2^*$. For $m_1^* > m_2^*$, the case in Fig. 5(a), the results are

$$I_{3D,CLM}/A = \frac{q}{4\pi^3}\int_{\sqrt{2m_1^*\phi_B/\hbar}}^\infty dkk^2 \int_0^{\sin^{-1}\sqrt{m_2^*/m_1^*\times(1-2m_1^*\phi_B/\hbar^2k^2)}} d\theta \sin\theta \int_0^{2\pi} d\phi \frac{\hbar k}{m_1^*}\cos\theta f_0 = \frac{qm_2^*}{2\pi^2\hbar^3}(k_BT)^2\mathcal{F}_1(\eta_F), \tag{A2a}$$

$$I_{q,3D,CLM}/A = \frac{1}{4\pi^3}\int_{\sqrt{2m_1^*\phi_B/\hbar}}^\infty dkk^2 \int_0^{\sin^{-1}\sqrt{m_2^*/m_1^*\times(1-2m_1^*\phi_B/\hbar^2k^2)}} d\theta \sin\theta \int_0^{2\pi} d\phi (E - E_F)\frac{\hbar k}{m_1^*}\cos\theta f_0 = \frac{m_2^*}{2\pi^2\hbar^3}(k_BT)^3[2\mathcal{F}_2(\eta_F) - \eta_F\mathcal{F}_1(\eta_F)], \tag{A2b}$$

and we note that the results of Eq. (A2) are the same as those from Eq. (A1). In Fig. 5(a), the hyperbola (A) that maps onto the k_x-k_y plane with $k_z=0$ (A′) on the barrier is expressed as

$$\frac{\hbar^2k_z^2}{2m_1^*} - \left(\frac{m_1^*}{m_2^*} - 1\right)\frac{\hbar^2(k_x^2 + k_y^2)}{2m_1^*} = \phi_B. \tag{A3}$$

For $m_1^* < m_2^*$, the case in Figs. 6(a) and 7(a), I and I_q become

$$I_{3D,CLM}/A = \frac{q}{4\pi^3}\int_{\sqrt{2m_1^*\phi_B/\hbar}}^{\sqrt{2m_1^*\phi_B/\hbar}\times\sqrt{m_2^*/(m_2^*-m_1^*)}} dkk^2 \int_0^{\sin^{-1}\sqrt{m_2^*/m_1^*\times(1-2m_1^*\phi_B/\hbar^2k^2)}} d\theta \sin\theta \int_0^{2\pi} d\phi \frac{\hbar k}{m_1^*}\cos\theta f_0$$
$$+ \frac{q}{4\pi^3}\int_{\sqrt{2m_1^*\phi_B/\hbar}\times\sqrt{m_2^*/(m_2^*-m_1^*)}}^{\infty} dkk^2 \int_0^{\pi/2} d\theta \sin\theta \int_0^{2\pi} d\phi \frac{\hbar k}{m_1^*}\cos\theta f_0 = \frac{qm_2^*}{2\pi^2\hbar^3}(k_BT)^2\int_0^{m_1^*/(m_2^*-m_1^*)\times\phi_B/k_BT} dx\frac{x}{1+e^{x-\eta_F}}$$
$$+ \frac{qm_1^*}{2\pi^2\hbar^3}(k_BT)^2\int_{m_1^*/(m_2^*-m_1^*)\times\phi_B/k_BT}^{\infty} dx\frac{x+\phi_B/k_BT}{1+e^{x-\eta_F}}, \tag{A4a}$$

$$I_{q,3D,CLM}/A = \frac{1}{4\pi^3}\int_{\sqrt{2m_1^*\phi_B/\hbar}}^{\sqrt{2m_1^*\phi_B/\hbar}\times\sqrt{m_2^*/(m_2^*-m_1^*)}} dkk^2 \int_0^{\sin^{-1}\sqrt{m_2^*/m_1^*\times(1-2m_1^*\phi_B/\hbar^2k^2)}} d\theta \sin\theta \int_0^{2\pi} d\phi(E-E_F)\frac{\hbar k}{m_1^*}\cos\theta f_0$$
$$+ \frac{1}{4\pi^3}\int_{\sqrt{2m_1^*\phi_B/\hbar}\times\sqrt{m_2^*/(m_2^*-m_1^*)}}^{\infty} dkk^2 \int_0^{\pi/2} d\theta \sin\theta \int_0^{2\pi} d\phi(E-E_F)\frac{\hbar k}{m_1^*}\cos\theta f_0$$
$$= \frac{m_2^*}{2\pi^2\hbar^3}(k_BT)^3\int_0^{m_1^*/(m_2^*-m_1^*)\times\phi_B/k_BT} dx\frac{(x-\eta_F)x}{1+e^{x-\eta_F}} + \frac{m_1^*}{2\pi^2\hbar^3}(k_BT)^3\int_{m_1^*/(m_2^*-m_1^*)\times\phi_B/k_BT}^{\infty} dx\frac{(x-\eta_F)(x+\phi_B/k_BT)}{1+e^{x-\eta_F}}. \tag{A4b}$$

As $m_1^*/(m_2^*-m_1^*)\times\phi_B/k_BT\to\infty$ ($m_1^*<\sim m_2^*$ or $\phi_B\gg k_BT$), we note that Eq. (A4) approaches to Eq. (A1), and the model becomes equivalent to the TOB model as shown in Fig. 6(a). As $m_1^*/(m_2^*-m_1^*)\times\phi_B/k_BT\to 0$ ($m_1^*\ll m_2^*$ with low ϕ_B), however, Eq. (A4) is different from the TOB model as shown in Fig. 7(a). In Figs. 6(a) and 7(a), the ellipsoid (A) that maps onto the k_x-k_y plane with $k_z=0$ (A′) on the barrier is expressed as Eq. (A3). In Fig. 7(a), the k_x-k_y plane with $k_z=0$ (B) in the well maps onto a hyperbola (B′) on the barrier, which is given as

$$-\frac{\hbar^2k_z^2}{2m_2^*} + \left(1-\frac{m_1^*}{m_2^*}\right)\frac{\hbar^2(k_x^2+k_y^2)}{2m_1^*} = \phi_B. \tag{A5}$$

In the NCLM model, I and I_q for 3D carriers are

$$I_{3D,NCLM}/A = \frac{q}{4\pi^3}\int_{\sqrt{2m_1^*\phi_B/\hbar}}^{\infty} dkk^2 \int_0^{\pi/2} d\theta \sin\theta \int_0^{2\pi} d\phi \frac{\hbar k}{m_1^*}\cos\theta f_0 = \frac{qm_1^*}{2\pi^2\hbar^3}(k_BT)^2\left[\mathcal{F}_1(\eta_F) + \frac{\phi_B}{k_BT}\mathcal{F}_0(\eta_F)\right], \tag{A6a}$$

$$I_{q,3D,NCLM}/A = \frac{1}{4\pi^3}\int_{\sqrt{2m_1^*\phi_B/\hbar}}^{\infty} dkk^2 \int_0^{\pi/2} d\theta \sin\theta \int_0^{2\pi} d\phi(E-E_F)\frac{\hbar k}{m_1^*}\cos\theta f_0 = \frac{m_1^*}{2\pi^2\hbar^3}(k_BT)^3\left[2\mathcal{F}_2(\eta_F) + \left(\frac{\phi_B}{k_BT}-\eta_F\right)\mathcal{F}_1(\eta_F)\right.$$
$$\left. - \frac{\phi_B}{k_BT}\eta_F\mathcal{F}_0(\eta_F)\right], \tag{A6b}$$

and by comparing Eqs. (A1) and (A6), we can show that $f(E)$ on the barrier should satisfy $f(E)=E/(E-\phi_B)\times f_0(E)$ to be consistent with the NCLM model for 3D homojunctions. The relation for 2D carriers $f(E)=\sqrt{E/(E-\phi_B)}\times f_0(E)$ can be obtained in a similar way. Note that $f(E)>f_0(E)$, and $f(E)$ can be even larger than 1 in the NCLM model.

[1] G. D. Mahan, J. Appl. Phys. **76**, 4362 (1994).
[2] G. D. Mahan, J. O. Sofo, and M. Bartkowiak, J. Appl. Phys. **83**, 4683 (1998).
[3] G. D. Mahan and L. M. Woods, Phys. Rev. Lett. **80**, 4016 (1998).
[4] A. Shakouri, E. Y. Lee, D. L. Smith, V. Narayanamurti, and J. E. Bowers, Microscale Thermophys. Eng. **2**, 37 (1998).
[5] T. Zeng and G. Chen, Microscale Thermophys. Eng. **4**, 39 (2000).
[6] D. Vashaee and A. Shakouri, Phys. Rev. Lett. **92**, 106103 (2004).
[7] D. Vashaee and A. Shakouri, J. Appl. Phys. **95**, 1233 (2004).
[8] M. D. Ulrich, P. A. Barnes, and C. B. Vining, J. Appl. Phys. **90**, 1625 (2001).
[9] H. J. Goldsmid, *Thermoelectric Refrigeration* (Plenum, New York, 1964).
[10] A. Shakouri, Proceedings of the 24th International Conference on Thermoelectrics (2005), pp. 507–512.
[11] C. B. Vining and G. D. Mahan, J. Appl. Phys. **86**, 6852 (1999).
[12] T. E. Humphrey, M. F. O'Dwyer, C. Zhang, and R. A. Lewis, J. Appl. Phys. **98**, 026108 (2005).
[13] Z. Bian and A. Shakouri, Appl. Phys. Lett. **88**, 012102 (2006).
[14] Z. Bian and A. Shakouri, *Nonequilibrium Carrier Dynamics in Semiconductors* (Springer, Berlin, 2006), pp. 179–182.
[15] S. Wang and N. Mingo, Phys. Rev. B **79**, 115316 (2009).
[16] A. Rahman, G. Jing, S. Datta, and M. S. Lundstrom, IEEE Trans. Electron Devices **50**, 1853 (2003).
[17] S. M. Sze and K. K. Ng, *Physics of Semiconductor Devices*, 3rd ed. (Wiley, New York, 2007).
[18] S. Datta, *Quantum Transport: Atom to Transistor* (Cambridge University Press, New York, 2005).
[19] Z. Ren, Ph.D. thesis, Purdue University, 2001.
[20] J. S. Blakemore, Solid-State Electron. **25**, 1067 (1982).
[21] R. Kim and M. Lundstrom, *Notes on Fermi-Dirac Integrals*, 3rd ed., http://nanohub.org/resources/5475 (2008).
[22] C. M. Wu and E. S. Yang, Solid-State Electron. **22**, 241 (1979).
[23] K. Yang, J. R. East, and G. I. Haddad, Solid-State Electron. **36**, 321 (1993).
[24] K. Horio and H. Yanai, IEEE Trans. Electron Devices **37**, 1093 (1990).
[25] R. Stratton, Phys. Rev. **125**, 67 (1962).
[26] C. R. Crowell, Solid-State Electron. **12**, 55 (1969).

[27]C. R. Crowell and V. L. Rideout, Solid-State Electron. **12**, 89 (1969).
[28]T. Low, S. Hong, J. Appenzeller, S. Datta, and M. S. Lundstrom, IEEE Trans. Electron Devices **56**, 1292 (2009).
[29]R. Kim, S. Datta, and M. S. Lundstrom, J. Appl. Phys. **105**, 034506 (2009).
[30]D. L. Smith, E. Y. Lee, and V. Narayanamurti, Phys. Rev. Lett. **80**, 2433 (1998).
[31]D. L. Smith, M. Kozhevnikov, E. Y. Lee, and V. Narayanamurti, Phys. Rev. B **61**, 13914 (2000).
[32]M. Kozhevnikov, V. Narayanamurti, C. Zheng, Y.-J. Chiu, and D. L. Smith, Phys. Rev. Lett. **82**, 3677 (1999).
[33]B. Moyzhes and V. Nemchinsky, Appl. Phys. Lett. **73**, 1895 (1998).
[34]H. A. Bethe, MIT Radiation Laboratory Report No. 43-12, 1942.
[35]F. Berz, Solid-State Electron. **28**, 1007 (1985).
[36]M. V. Fischetti, L. Wang, B. Yu, C. Sachs, P. M. Asbeck, Y. Taur, and M. Rodwell, Proceedings of the Electron Devices Meeting (2007), pp. 109–112.
[37]M. V. Fischetti, S. Jin, T.-w. Tang, P. Asbeck, Y. Taur, S. E. Laux, M. Rodwell, and N. Sano, J. Comput. Electron. **8**, 60 (2009)
[38]R. J. Radtke, H. Ehrenreich, and C. H. Grein, J. Appl. Phys. **86**, 3195 (1999).

AIP | Journal of Applied Physics

On momentum conservation and thermionic emission cooling

Raseong Kim, Changwook Jeong, and Mark S. Lundstrom

Citation: Journal of Applied Physics **107**, 054502 (2010); doi: 10.1063/1.3295899
View online: http://dx.doi.org/10.1063/1.3295899
View Table of Contents: http://scitation.aip.org/content/aip/journal/jap/107/5?ver=pdfcov
Published by the AIP Publishing